Intermediate Report: Multi-Fidelity Bayesian Optimization for Wind Farm Layout Optimization

Aman Choudhri (ac4972)

January 15, 2025

1 Methods

1.1 Problem Setup

Let $X \in \mathbb{R}^{N \times 2}$ represent the locations of N wind turbines. For a given incoming wind speed v at direction ϕ, write the power produced by the farm (as estimated by a large eddy simulation) as $f_{\text{LES}}(X, v, \phi)$

Our ultimate objective of interest is the expected power production of a wind farm over a historical wind condition distribution $p(v, \phi)$. We write this objective as

$$g_p(X) := \mathbb{E}_{p(v,\phi)}[f_{\text{LES}}(X, v, \phi)].$$

Denote our analytic approximation to the "true" power production f_{LES} by f_{approx}. Our goal is to solve the above optimization problem given a fixed evaluation budget, where we assume fixed evaluation costs for each fidelity, c_{LES} and c_{approx}.

To simplify the computation for this paper, we fix one incoming wind condition v, ϕ, solving:

$$\begin{aligned} \text{maximize}_X \quad & f_{\text{LES}}(X, v, \phi) \\ \text{subject to} \quad & x_i \in \Omega \quad \forall i \in \{1, \dots, N\} \end{aligned}$$

where Ω represents the available land area for the wind farm.

1.2 Optimization Approach

In this work, we follow the multi-task BO (MTBO) approach introduced in [12] and shown in [7] to be successful for regimes where one observation model is significantly more expensive to evaluate.

Specifically, the different evaluation modes, f_{approx} and f_{LES} are modeled using the intrinsic model of coregionalization (ICM). Specifically, it posits two underlying independent Gaussian processes,

$$h_1, h_2 \sim_{\text{iid}} \mathcal{GP}(0, \kappa),$$

that are linearly mixed to yield the observation modes as

$$\begin{aligned} f_{\text{approx}} &= a^{(1)}_{\text{approx}} h_1 + a^{(2)}_{\text{approx}} h_2 \\ f_{\text{LES}} &= a^{(1)}_{\text{LES}} h_1 + a^{(2)}_{\text{LES}} h_2. \end{aligned}$$

The mixing coefficients a are learned by maximizing marginal log likelihood along with kernel hyperparameters. In this paper, we use the ARD Matern kernel with smoothness $\nu = 5/2$.

The acquisition function for this model is noiseless batch expected improvement (qEI), with incumbents defined over LES observations only. For a batch size of B, this is given by

$$\alpha(X|D_{\text{LES}}, D_{\text{GCH}}) = \mathbb{E}\left[\max_{i=1,\ldots,B} \max\left(0, f_{\text{LES}}(X_i) - f^*_{\text{LES}}\right) \;\middle|\; D_{\text{LES}} \cup D_{\text{GCH}}\right],$$

for incumbent f^*_{LES} defined as $\max_{x \in D_{\text{LES}}} f_{\text{LES}}(x)$. To simplify the implementation, the reference paper [7] alternates using this acquisition function to pick batches for the cheap and expensive observation models, with different batch sizes for each. We follow this design, trading off batches evaluated using GCH and LES.

We do make one notable change relative to the MTBO paper: namely, we acquire and observe the cheap evaluations within a "batch" sequentially. This does incur a cost overhead for more acquisition function maximizations. The hope was that the expensive LES computation would dominate the optimization procedure runtime, meaning this extra acquisition overhead would be negligible and yield essentially free performance improvement.

2 Results

We optimized the placement of only $N = 4$ turbines as a proof of concept (by comparison, the authors of [3] picked $N = 16$) This limits the difficulty of the optimization problem and the cost of running large eddy simulations, but include enough turbines that wake effects would be non-negligible.

For our turbines, we employed the commonly-used `NREL-5MW` [6] reference turbine specification. The turbines have a diameter of $D = 126m$ and a hub height of $90m$.

2.1 Wind Farm Simulations

Large-eddy simulations were conducted on a grid of size $L_x \times L_y \times L_z = 2004m \times 504m \times 1336m$, where y represents the vertical direction. Due to computational limitations, we employ a relatively coarse spatial discretization with mesh size $N_x \times N_y \times N_z = 100 \times 51 \times 72$. This corresponds to a horizontal resolution of approximately $20m$ ($\Delta x = 20.04m, \Delta z = 18.85m$) and a vertical resolution of $\Delta y = 9.88m$. Similar papers [3, 10] employed a uniform mesh resolution of approximately $10m$ in all directions. Recent papers exploring the utility of large eddy simulation for real-time wind farm control have found that grid resolutions as coarse as $80m$ horizontally can still meaningfully simulate total wind farm power output, so we maintain that the resolution is not a significant limitation of this work [5].

A temporal resolution of $\Delta t = 0.2s$ was employed, following similar papers [10, 3].

To ensure proper modeling of turbulent wind flow in the atmospheric boundary layer (ABL), it is common to employ a precursor simulation, a separate LES run without turbines whose output velocity planes are used as the inflow conditions to the real wind farm LES [8, 4, 11].

The ABL was simulated with friction velocity $u^* = 0.442m/s$, height $\delta = 504m$, and roughness length $z_0 = 0.05m$, following [2]. The resulting simulated ABL inflow exhibited a mean streamwise velocity at the turbine hub height of $U_h = 9.48m/s$, with a turbulence intensity at the same height of $TI = 7.2\%$. Figure 1 displays the full simulated wind profiles.

A moderate deviation is observed in the streamwise velocity relative to the "log law" profile expected from similar simulations of neutral ABLs [1, pg. 191]. The deviation is likely due to the relatively coarse computational mesh employed in this paper. See Figures A.1 and A.2 for ABL profiles simulated under coarser and finer meshes.

The large eddy simulations were run for a 30 minute spinup period, and power output was averaged over a subsequent 2 hour period. Figure 2 displays the trajectory of the simulated power

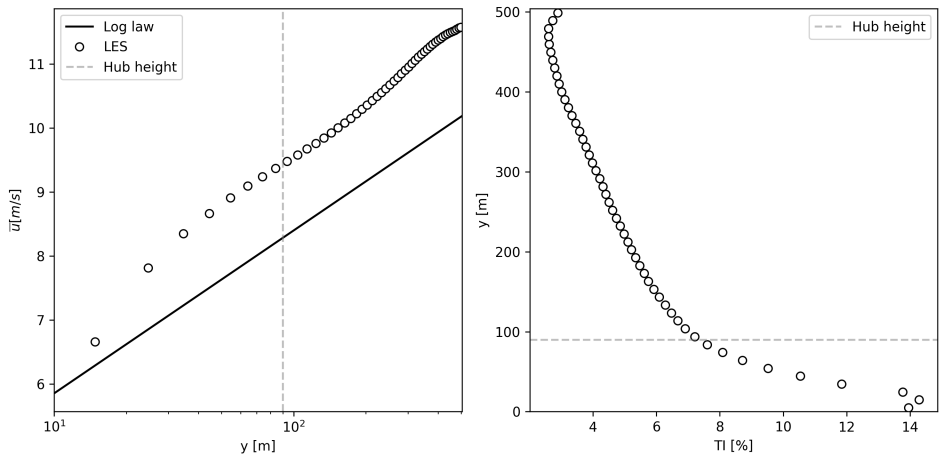

Figure 1: Mean streamwise velocity (left) and turbulence intensity (right) of the simulated atmospheric boundary layer

output over this two hour period, showing that the cumulative average power output stabilizes relatively quickly, between 30 and 60 minutes after spinup. This suggests that we may see significant efficiency gains from an adaptive approach wherein the simulation duration is varied by the optimization campaign.

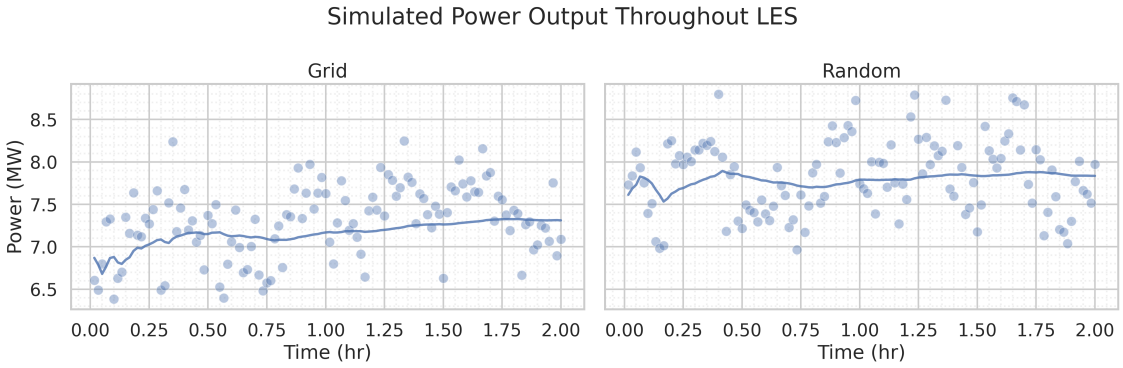

Figure 2: Statistical convergence of simulated wind farm power output in both a grid and random turbine layout. All measurements were taken after a 30 minute spinup period.

2.2 Layout Optimization

To allow for the kernel hyperparameters to be fit, we initialize the optimization routine with $K_{\text{approx}} = 100$ prefixed evaluations from the GCH approximation model, and $K_{\text{LES}} = 12$ from the large-eddy simulation, following [10]. The initial layouts were sampled using Latin hypercube sampling, along with an additional default layout of the turbines placed in an evenly spaced grid. Figure 3 displays mean and instantaneous velocity simulations for the grid layout.

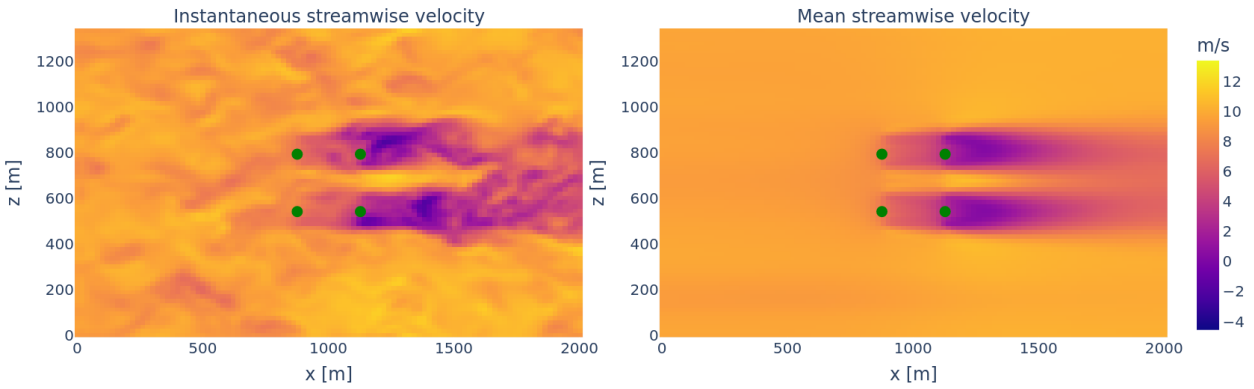

Figure 3: Instantaneous (left) and mean (right) streamwise velocity field for a grid farm layout, with wind flowing in the positive x direction. The instantaneous field was saved 1 hour after the 30 minute spinup period.

2.3 Single-Fidelity Layout Optimization with LES

As a baseline for comparison for the multi-fidelity layout optimization run, we performed a single-fidelity BO campaign with large eddy simulation evalutions only. To increase throughput and reduce the wall-clock time of each run, batch optimization was performed, with $B = 5$ simulations run in parallel at each optimization step. The procedure was run for 48 hours, resulting in 56 completed batches.

Figure 4 displays the optimization history of this LES-only run. The best performing layout the optimization routine identifies achieves a power production of 14.9 MW.

2.4 Multi-Fidelity Layout Optimization

The multi-fidelity layout optimization run was performed by alternating evaluation batches between GCH and LES observations, as described in Section 1.2. At each step, we employed batch sizes of $B_{\text{GCH}} = 50$ and $B_{\text{LES}} = 4$. The power trajectory for this optimization run is also displayed in Figure 5.

Again, this layout optimization procedure was allowed 24 hours to run. It was able to complete 21 full evaluation rounds, totaling 525 GCH evaluations and 84 LES evaluations.

The best layout found by the multi-fidelity campaign is slightly worse than the best found by the single-fidelity campaign, at 14.6 MW.

The multi-fidelity campaign is able to find a near-final layout achieving 14.5 MW within the first 4 large eddy simulation batches. By contrast, the single-fidelity campaign does not find a configuration producing more than 14 MW until the 12th batch. As expected, having access to the GCH evaluation fidelity significantly speeds up optimization progression. This result raises the interesting question of how the performance difference might change under a more difficult layout optimization problem with more turbines, a regime where sample efficiency may be far more important.

3 Discussion

This work demonstrates the potential benefits of multi-fidelity Bayesian optimization for wind farm layout optimization, while also highlighting several promising directions for future research.

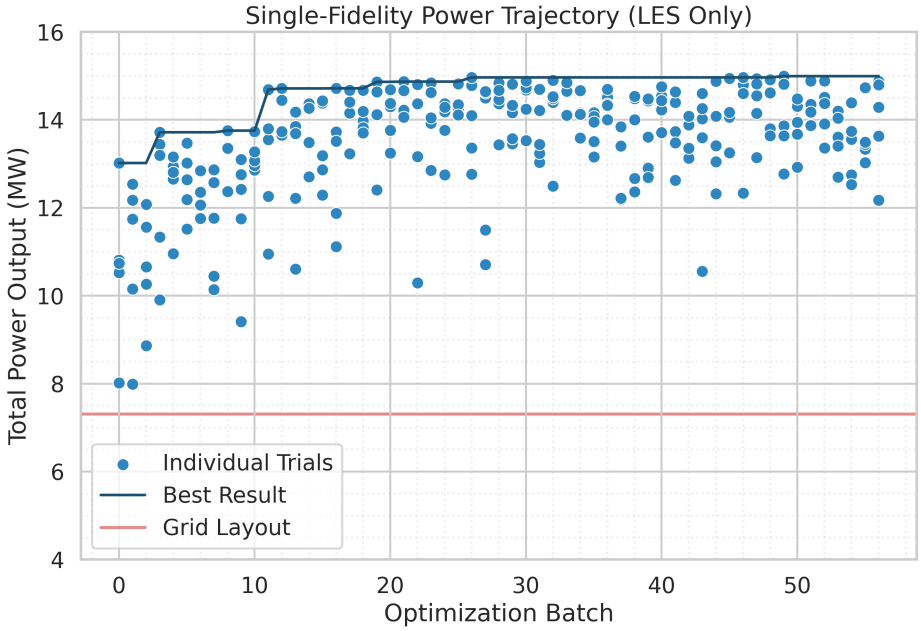

Figure 4: Wind farm configuration power output throughout single-fidelity (LES only) Bayesian layout optimization. For reference, the power production of a standard grid wind farm layout is displayed in red.

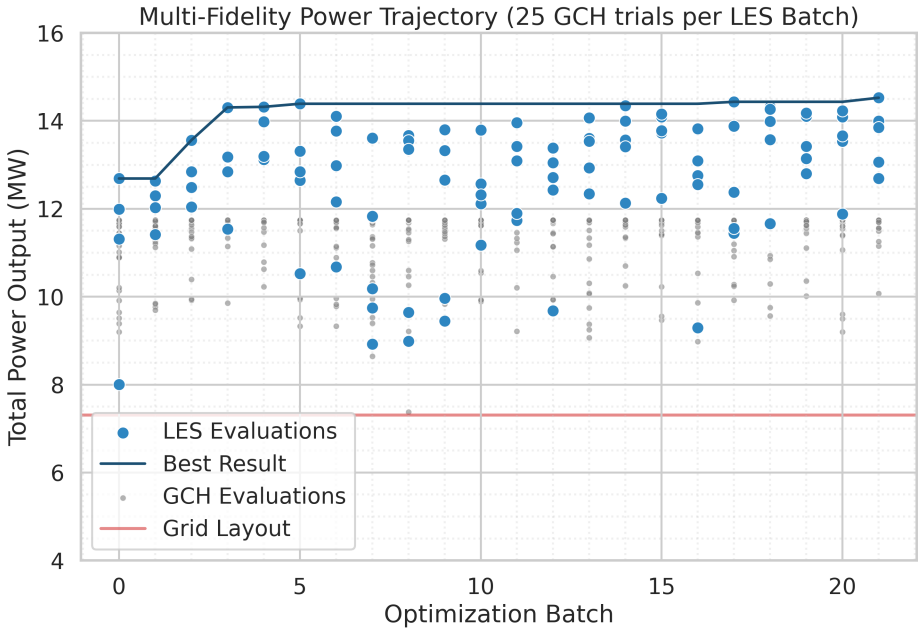

Figure 5: Wind farm configuration power output throughout multi-fidelity Bayesian layout optimization. Low-fidelity approximate evaluations using GCH are shown in grey, and expensive high-fidelity LES evaluations are shown in blue. For reference, the power production of a standard grid wind farm layout is displayed in red.

First, our results suggest that multi-fidelity optimization can achieve near-optimal layouts with significantly fewer expensive LES evaluations compared to single-fidelity approaches. However, the current study's limitation to just four turbines leaves open the question of how these benefits scale to more realistic wind farm configurations. We hypothesize that the sample efficiency gains from multi-fidelity optimization will become even more pronounced as the dimensionality of the layout optimization problem increases.

Several methodological extensions could significantly improve the practical utility of this approach:

1. **Adaptive Fidelity Selection:** Rather than manually alternating between GCH and LES evaluations, implementing cost-aware acquisition functions (like that of [13]) could automatically balance the exploration-exploitation trade-off across fidelities.

2. **Variable Wind Conditions:** The current work considers only a single inflow wind direction and speed. Extending the optimization to handle varying inflowing wind speeds and directions would better reflect real-world conditions.

3. **Adaptive LES Duration:** Our convergence analysis (Figure 2) suggests that power output statistics stabilize relatively quickly. This opens the possibility of adaptively selecting simulation durations, potentially reducing computational cost without sacrificing accuracy. Early optimization iterations might use shorter simulations, with longer durations reserved for promising configurations.

4. **Grey-box Optimization:** Currently, we treat each LES evaluation as a black box, only observing the final time-averaged power output. However, the LES solver produces rich intermediate results throughout its run, including instantaneous power measurements and velocity field data. A grey-box Bayesian optimization approach could leverage these intermediate observations to make early stopping decisions or guide the selection of subsequent layouts, potentially yielding significant efficiency improvements.

4 Code Availability

The implementation of the methods described in this paper, including optimization routines and simulation configurations, is available at https://github.com/amanchoudhri/windopt.

5 Acknowledgements

Major thanks to Prof. Nikos Bempedelis of Queen Mary University of London for his detailed guidance on large eddy simulation configuration and BO approaches to the layout optimization problem. A further thanks to Prof. John Cunningham of Columbia for his instruction on Bayesian Optimization during Columbia's STAT6103 Applied Statistics course, and his help on the framing of this paper and shaping the future directions of the methods explored.

References

[1] S. Pal Arya. *Introduction to Micrometeorology*. 2nd ed. This Is Volume 79 in the International Geophysics Series. San Diego: Academic Press, 2001. ISBN: 978-0-12-059354-5.

[2] Nikolaos Bempedelis and Luca Magri. "Bayesian Optimization of the Layout of Wind Farms with a High-Fidelity Surrogate Model". In: *Computational Science – ICCS 2023*. Ed. by Jiří Mikyška et al. Cham: Springer Nature Switzerland, 2023, pp. 344–352. ISBN: 978-3-031-36027-5. DOI: 10.1007/978-3-031-36027-5_26.

[3] Nikolaos Bempedelis et al. "Data-Driven Optimisation of Wind Farm Layout and Wake Steering with Large-Eddy Simulations". In: *Wind Energy Science* 9.4 (Apr. 2024), pp. 869–882. ISSN: 2366-7451. DOI: 10.5194/wes-9-869-2024. (Visited on 11/15/2024).

[4] A. Ferrante and S. E. Elghobashi. "A Robust Method for Generating Inflow Conditions for Direct Simulations of Spatially-Developing Turbulent Boundary Layers". In: *J. Comput. Phys.* 198.1 (July 2004), pp. 372–387. ISSN: 0021-9991. DOI: 10.1016/j.jcp.2004.01.016. (Visited on 12/10/2024).

[5] Nick Janssens and Johan Meyers. "Towards Real-Time Optimal Control of Wind Farms Using Large-Eddy Simulations". In: *Wind Energy Science* 9.1 (Jan. 2024), pp. 65–95. ISSN: 2366-7443. DOI: 10.5194/wes-9-65-2024. (Visited on 12/10/2024).

[6] J. Jonkman et al. *Definition of a 5-MW Reference Wind Turbine for Offshore System Development*. Tech. rep. NREL/TP-500-38060, 947422. Feb. 2009, NREL/TP-500–38060, 947422. DOI: 10.2172/947422. (Visited on 12/12/2024).

[7] Benjamin Letham and Eytan Bakshy. "Bayesian Optimization for Policy Search via Online-Offline Experimentation". In: *Journal of Machine Learning Research* 20.145 (2019), pp. 1–30. ISSN: 1533-7928. (Visited on 12/27/2024).

[8] Thomas S. Lund, Xiaohua Wu, and Kyle D. Squires. "Generation of Turbulent Inflow Data for Spatially-Developing Boundary Layer Simulations". In: *Journal of Computational Physics* 140.2 (Mar. 1998), pp. 233–258. ISSN: 0021-9991. DOI: 10.1006/jcph.1998.5882. (Visited on 12/10/2024).

[9] P. J. Mason and D. J. Thomson. "Stochastic Backscatter in Large-Eddy Simulations of Boundary Layers". In: *Journal of Fluid Mechanics* 242 (Sept. 1992), pp. 51–78. ISSN: 1469-7645, 0022-1120. DOI: 10.1017/S0022112092002271. (Visited on 12/31/2024).

[10] Andrew Mole and Sylvain Laizet. *Multi-Fidelity Bayesian Optimisation of Wind Farm Wake Steering Using Wake Models and Large Eddy Simulations*. July 2024. arXiv: 2407.20832 [physics]. (Visited on 11/15/2024).

[11] Richard J. A. M. Stevens, Jason Graham, and Charles Meneveau. "A Concurrent Precursor Inflow Method for Large Eddy Simulations and Applications to Finite Length Wind Farms". In: *Renewable Energy* 68 (Aug. 2014), pp. 46–50. ISSN: 09601481. DOI: 10.1016/j.renene.2014.01.024. arXiv: 1405.0980 [physics]. (Visited on 12/10/2024).

[12] Kevin Swersky, Jasper Snoek, and Ryan P Adams. "Multi-Task Bayesian Optimization". In: *Advances in Neural Information Processing Systems*. Vol. 26. Curran Associates, Inc., 2013. (Visited on 12/31/2024).

[13] Jian Wu et al. *Practical Multi-fidelity Bayesian Optimization for Hyperparameter Tuning*. Mar. 2019. DOI: 10.48550/arXiv.1903.04703. arXiv: 1903.04703 [cs]. (Visited on 01/12/2025).

A Large-Eddy Simulations

A.1 Configuration and Parameters

The classic Smagorinsky subgrid scale model was used, with the Smagorinsky constant taken as $\kappa = 0.14$. Wall damping was used according to the Mason and Thomson formulation [9], with a damping growth parameter of $n = 3$.

The forward timesteps were calculated using a third-order Runge-Kutta scheme. Simulations were run with inflow/outflow boundary conditions in the streamwise direction, periodic conditions in the spanwiise direction, and free-slip conditions in the vertical direction.

The actuator disks were modeled using the following common parameters:

Table A.1: Actuator Disk Parameters

Parameter	Value
Axial induction factor, a	0.25
Thrust coefficient, C_T	0.75

A.2 Precursor Simulations

The precursor simulation was run for a total of $72,000$ timesteps, or 4 hours. Outflow velocity planes were collected and saved following a 2 hour (7200 timestep) spinup period.

A moderate deviation from the log law profile expected under a simulation of a neutral ABL is observed in Figure 1. This deviation is likely due to the horizontal resolution of the computational mesh used in the precursor simulation, at $\Delta x \approx \Delta z \approx 20m$. Figures A.1 and A.2 illustrate this point, displaying profiles for ABLs simulated under other horizontal mesh resolutions.

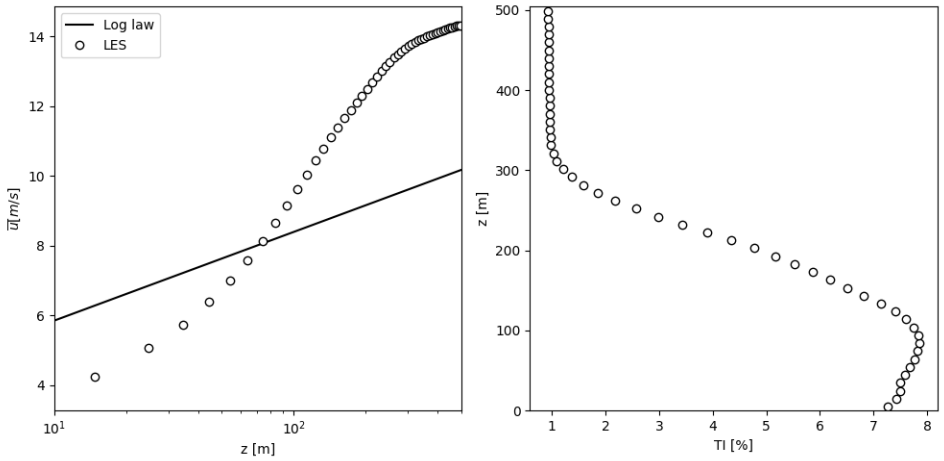

Figure A.1: Precursor ABL Profile for Coarser Horizontal Mesh Resolution, $\Delta x = \Delta z = 40m$

B Computational Details

Large-eddy simulations were computed via parallelization across 8 nodes of Columbia's Terremoto cluster. Each node has two 12-core CPUs, for a total of 192 cores involved in computing each

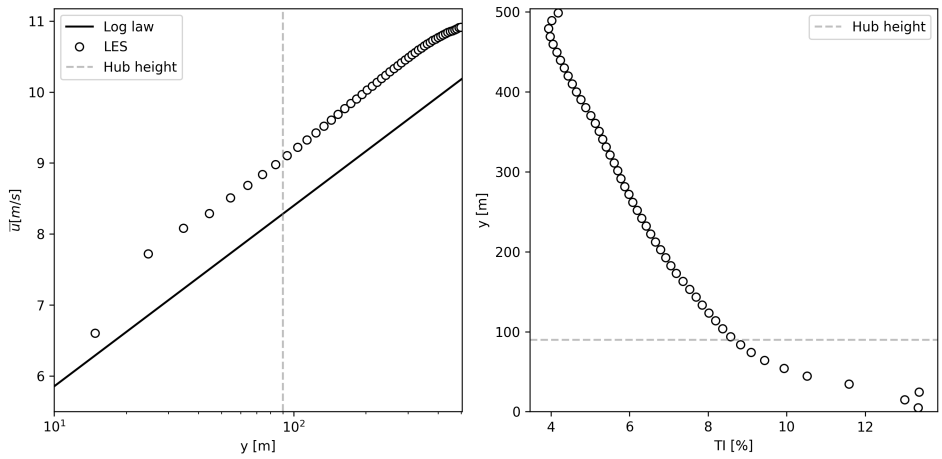

Figure A.2: Precursor ABL Profile for Finer Horizontal Mesh Resolution, $\Delta x = \Delta z = 10m$

simulation. The CPUs used were Intel Xeon Gold 6127 2.6 GHz processors.

Under this configuration, the scaling time of the large-eddy simulations was roughly 2.5 simulated wind farm seconds per wall-clock second.